Environmental Engineering and Management Journal

August 2020, Vol. 19, No.8, 1275-1287
http://www.eemj.icpm.tuiasi.ro/; http://www.eemj.eu

"Gheorghe Asachi" Technical University of Iasi, Romania

FORECASTING OF CHLOROPHENOLS REMOVING WITH ADVANCED OXIDATION PROCESSES: AN ARTIFICIAL NEURAL NETWORKS APPLICATION

Aysun Altikat[1*], Zeynep Ceylan[2], Alper Gulbe[3]

[1]Iğdır University Engineering Faculty Department of Environmental Engineering, Iğdır, 76000, Turkey
[2]Atatürk University Engineering Faculty Department of Environmental Engineering, Erzurum, 25240, Turkey
[3]Iğdır University, Technical Sciences Vocational School, Department of Computer Programming, Iğdır, 76000, Turkey

Abstract

Advanced oxidation processes (AOPs) are used with high efficiency in wastewater treatment due to the formation of hydroxyl radicals with high oxidation capacity. However, there exists many different variables which affect the efficiency of theses processes as it affects the amount of hydroxyl radicals formed; such as reaction time, pH, temperature, reactant concentrations and catalyst amount. In this study, the removal of 2-chlorophenol (2-CP) and 2,4-dichlorophenol (2,4-DCP), which are highly toxic organic pollutants, with Fenton oxidation was investigated. This research has two aims. The first is modelling of substituted phenols removing with AOPs utilizing artificial neural networks (ANN), and the second is determination of the relative important among the input parameters for removing. In the research, 18 different ANN structures were used. The best ANN model for prediction of 2-CP and chemical oxygen demand from 2-CP ($COD_{2\text{-}CP}$) were determined at the ANN10 structure. In this structure, 15 neurons, Levenberg-Marquardt and logarithmic sigmoid-symmetric sigmoid were used as learning and transfer functions, respectively. In addition, at the ANN16 and ANN2 structures, which were used for the prediction of removing efficiency for 2,4-DCP and $COD_{2,4\text{-}DCP}$, have obtained better results. In both models, Levenberg-Marquardt learning function was used. In ANN16, transfer functions were logarithmic sigmoid-symmetric sigmoid with 20 neurons and, in ANN2, symmetric sigmoid-symmetric sigmoid transfer functions with 10 neurons. When examined the sensitivity analysis results, all the input parameters have a significant effect on the substituted phenols removing with AOPs.

Key words: 2-chlorophenol, 2,4-dichlorophenol, artificial neural network, Fenton oxidation, modeling

Received: November, 2019; Revised final: March, 2020; Accepted: April, 2020; Published in final edited form: August, 2020

1. Introduction

Reuse of wastewater is an important issue in terms of the sustainable life cycle. Removing pollutants is necessary for the reuse of wastewater. One of the most effective method used in this treating process is the advanced oxidation processes (AOPs). Most of the pollutants are effectively removed from the wastewater by AOPs (Ameta, 2018). One of the most important of these pollutants is chlorophenols. Chlorophenols are used in many industries as raw materials (in the production of antiseptics and pesticides), intermediates (in bleaching for the papermaking industry, during chlorine disinfection of drinking water and wastewater) (Olaniran and Igbinosa, 2011) or product (as a result of microbial disintegration of herbicides and pesticides such as 2,4-dichlorophenoxyacetic acid and 2,4,5-trichlorophenoxyacetic acid which are also used in the food industry) (Badanthadka and Mehendale, 2014). Chlorophenols are used extensively as pesticides due to their toxic effects. Many types of chlorophenol are used to destroy harmful plants, fungi, mollusks, mites, bacteria and molds. Due to these wide usages, they

* Author to whom all correspondence should be addressed: e-mail: aysun.altikat@igdir.edu.tr; Phone: +90 476 223001, 4453

release into the environment and cause serious ecological problems in the area where they are discharged (Igbinosa et al., 2013). Oxidation with Fenton's reagent is based on hydroxyl radicals produced by the catalytic (ferrous ions, Fe^{2+} as catalysts) decomposition of hydrogen peroxide (H_2O_2) in acidic solution (Duesterberg et al., 2008). Treating of wastewater by AOPs is highly sophisticated process owing to it was influenced both initial H_2O_2, Fe^{2+} concentrations and pH and temperature conditions.

Large amount of the H_2O_2 concentrations is accompanied by an increase in the degradation rate of the organics due to intense hydroxyl radicals ($OH^{\bullet}$) (Zhao et al., 2004). Except that, in some cases, raising the H_2O_2 concentration may not increase the rate of degradation of organics owing to scavenging of $OH^{\bullet}$ by H_2O_2 (Kavitha and Palanivelu, 2004). H_2O_2 should be included at the optimum concentration to avoid this adverse situation.

There are some factors that affect the optimum H_2O_2 concentration such as pollutant and iron concentration. There is a linear correlation between the decay rate of organic substances and the iron concentration to a certain concentration level. Generally, an increase in iron concentration, as in H_2O_2, increases the rate of deterioration of organics although the efficiency decreases above a certain iron concentration (Ameta et al., 2018). The pH values influence the generation of the $OH^{\bullet}$ radicals, and the degradation level of organics. In the researches it stated that the maximum AOPs activity was determined at the pH 3 level. At higher pH levels, reproduction of $OH^{\bullet}$ radicals accompanies a fall caused by the decrease of dissolved iron together with dissociation and auto-decomposition of H_2O_2 (Zhao et al., 2004). Moreover, at lower pH levels, efficiency of the oxidation is also lower (Ameta et al., 2018). There is a direct correlation between the temperature and the speed of the Fenton process up to 40 degrees (Gulkaya et al., 2006), but at the temperatures above 40°C H_2O_2 may be decomposed to oxygen and water (Nesheiwat and Swanson, 2000).

The AOPs are very difficult to explain with classical mathematical models due to its very complexity. Artificial neural network (ANN) may generally be used in many modeling researches perfectly (Prakash et al., 2008). It has a lot of advantages such as less time, more prediction ability, limited numbers of experiments (Pareek et al., 2002). ANN is a circuit of propagating nodes called neurons, interconnected to a mesh by a set of coefficients called weights. Neurons accept a number of input values, multiplies those values with weights, adds a constant value called bias, sums them up, and uses this summation as the argument for a single-valued transfer function resulting in the output of the neuron (Strik et al., 2005). The ANNs consist of several simple and highly interconnected neurons, processing data by their dynamic state responses to external inputs. The layers and neurons are used in this network. The ANNs can be single-layer as in shallow learning or multi-layer in deep learning.

Depending on the structural features of the problem, the neurons can be connected to the network in different ways (Pawul and Śliwka, 2016). In many articles about wastewater treatments has been reported applications of ANN. ANNs were confided in treatment of biological (Kundu et al., 2013; Moral et al., 2008) and physicochemical wastewater (Aber et al., 2007; Daneshvar et al., 2006; Alyani et al., 2019). However, when it comes to AOPs, ANN was applied in a limited number of studies (Oguz et al., 2008).

This study deals mainly with the determination of the best model for forecasting 2-chlorophenol (2-CP), 2-chlorophenol's chemical oxygen demand ($COD_{2\text{-}CP}$), 2,4-dichlorophenol (2,4-DCP), chemical oxygen demand of 2,4-DCP ($COD_{2,4\text{-}DCP}$) at the Fenton process as one of AOPs. For this purpose, different ANN structures were used such that 18 different ones were tested with 3 different neuron numbers (10, 15, 20) and 6 different transfer function combinations.

2. Material and methods

2.1. Chemicals

2-CP (5000 ppm stock), 2,4-DCP (1000 ppm stock), 4-aminoantipyrine, and potassium ferricyanide were purchased from Sigma-Aldrich. H_2O_2 (35%), iron (II) sulfate heptahydrate, sodium hydroxide (1 N stock), sulfuric acid (1 N stock), potassium iodide, potassium dichromate, mercury (II) sulfate, silver sulfate, and ammonia solution, were purchased from Merck. Ultrapure water (Millipore Milli-Q) was used for preparation and dilution of all solutions.

2.2. Reactor structure

The test reactor is a reactor which has glass observation chamber fitted with 2.5 L steel cage (Ø 20 cm). The reactor has different compartments where the dissolved oxygen and pH probe are immersed. In order to prevent any leakage, these compartments have been tightened with Teflon bolts. The chemicals have been added through the opening at the reactor's top. The samples have been taken from the tap under the reactor. The experimental set up was illustrated in Fig. 1.

2.3. H_2O_2 oxidation experiments

When examining the H_2O_2 oxidation of pollutant molecules, H_2O_2 needs were calculated by using the formula [$H_2O_2 \approx 2.12COD$] considering the COD values of the molecules (Bautista et al., 2007; Tengrui et al., 2007). The solutions were subjected to rapid stirring (160 rpm) with 5 minutes followed by slow stirring (60 rpm). Samples were taken at certain times after the initiation of the reaction and neutralized with NaOH first to stop the hydrogen peroxide reactivity. The samples were then immediately analyzed for COD, H_2O_2, and model contaminants (2-CP and 2.4-DCP).

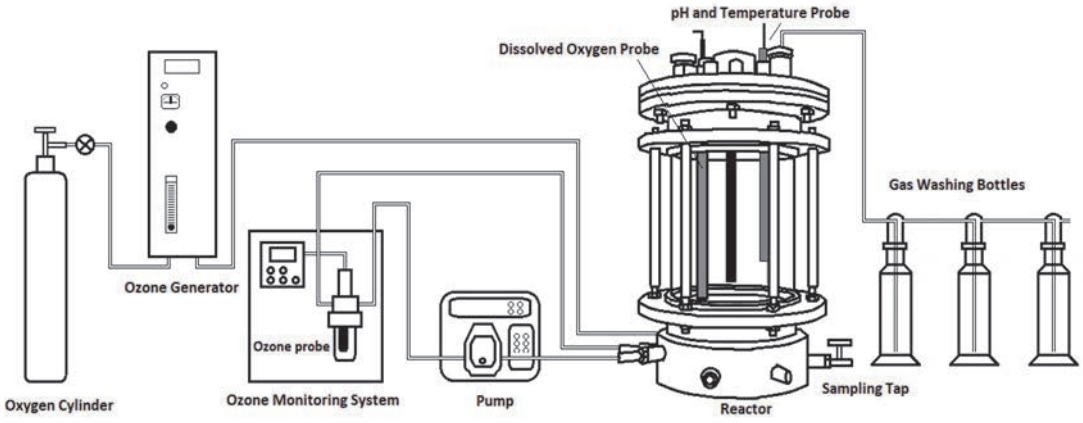

Fig. 1. Reactor structure

2.4. Fenton experiments

Generally, Fenton reaction mechanism depends on the formation of hydroxyl radicals as a result of the interaction of H_2O_2 and iron salts Eq. (1-5) (Ameta et al., 2018).

$$Fe^{2+} + H_2O_2 \rightarrow Fe^{3+} + OH^{\bullet} + OH^{-} \quad (1)$$

$$OH^{\bullet} + H_2O_2 \rightarrow HO_2^{\bullet} + H_2O \quad (2)$$

$$Fe^{3+} + HO_2^{\bullet} \rightarrow Fe^{2+} + H^{+} + O_2 \quad (3)$$

$$Fe^{2+} + HO_2^{\bullet} \rightarrow Fe^{3+} + HO_2^{-} \quad (4)$$

$$Fe^{2+} + OH^{\bullet} \rightarrow Fe^{3+} + OH^{-} \quad (5)$$

Although the reactive free hydroperoxyl radical ($HO_2^{\bullet}$-0.75 V) (Reitberger, 2001), molecular oxygen (O_2-1.23 V) and hydrogen peroxide (H_2O_2-1.78 V) formed in the above-mentioned reactions are also high, the highest oxidation potential belongs to the hydroxyl radical ($OH^{\bullet}$-2.86 V) (Rodríguez et al., 2008). Therefore, it is known that the main reagent responsible for degradation of organic pollutants almost to mineralization in AOPs are hydroxyl radicals.

2.5. Analysis procedures

For COD analysis, the pH of the samples was set to 7-8 and Fe^{2+} precipitated and separated by passing through 0.2 µm membrane filter tip syringe. In addition, H_2O_2 analysis was performed by iodometric method and the amount of H_2O_2 interfering with COD was determined. The pH values of the samples were determined by WTW Multi 340i multiparameter. Spectrophotometric analyzes such as H_2O_2 analysis, COD analysis, Fe^{2+} analysis, model pollutants analysis was performed on Shimadzu UV-160A spectrophotometer. COD analyzes were performed in Spectroquant TR420 thermoreactor at 148°C by the method specified in Standard Methods (APHA, 2017) and measured at 510 nm wavelength on the spectrophotometer. The model pollutants analysis was carried out according to the 4-aminoantipyrine method (Direct Photometric Method) described in the Standard Methods.

Analyzes were carried out at the wavelengths at which the optimal peaks occurred (464 nm for 2-CP, 510 nm for 2,4-DCP). In the literature, the 4-aminoantipyrine method developed for phenol and all its derivatives is frequently encountered (Lathasree et al., 2004). Hydrogen peroxide analysis is based on the reaction of H_2O_2 and iodide (I^{-}) ion to form triiodide (I_3^{-}) ion with absorbance value at 464 nm (Klassen et al., 1994). H_2O_2 interferes by reducing oxidative Cr^{6+} to Cr^{3+} in COD test. The following correction (Eq. 6) was used to prevent this intervention (Zak, 2008).

$$COD\,(real) = COD(measurement) - f \times [H_2O_2]\ (f = 0.25) \quad (6)$$

2.6. ANNs strategy

In the research, it was used 64 bits a computer (Windows 10) for ANN works. The computer has an NVIDIA GeForce 2 GB display card, Intel Core i7 - 6700 T CPU, 2.8 GHz processor and 8 GB of memory. In the ANNs structure, one learning function, 6 different transfer function combinations and 3 different numbers of neurons were used. The ANNs model, inputs and output parameters were illustrated in Fig. 2 while learning and transfer functions and neurons numbers which used in this research were given in Table 1. In addition, the ranges of the inputs were shown in Fig. 3.

2.7. Performance evaluation

The performance of constructed ANN models was statistically measured in terms of the root mean square error (*RMSE*) (Eq. 7), mean absolute error *(MAE) (*Eq. 8*)* and coefficient of determination, a.k.a. R-squared (R^2) (Eq. 9). R^2 is a number which confirms that the model fits well the data when it approaches to 1.0. RMSE is measurement of model's error rate and denotes the standard deviation of the model prediction error.

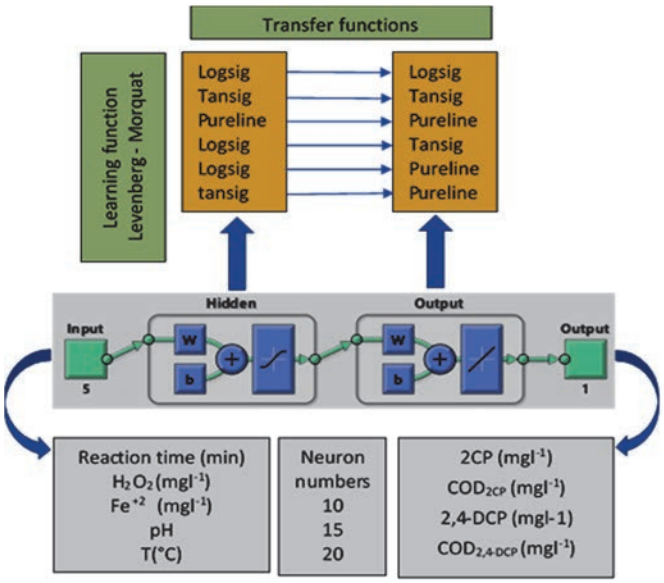

Fig. 2. ANNs structure

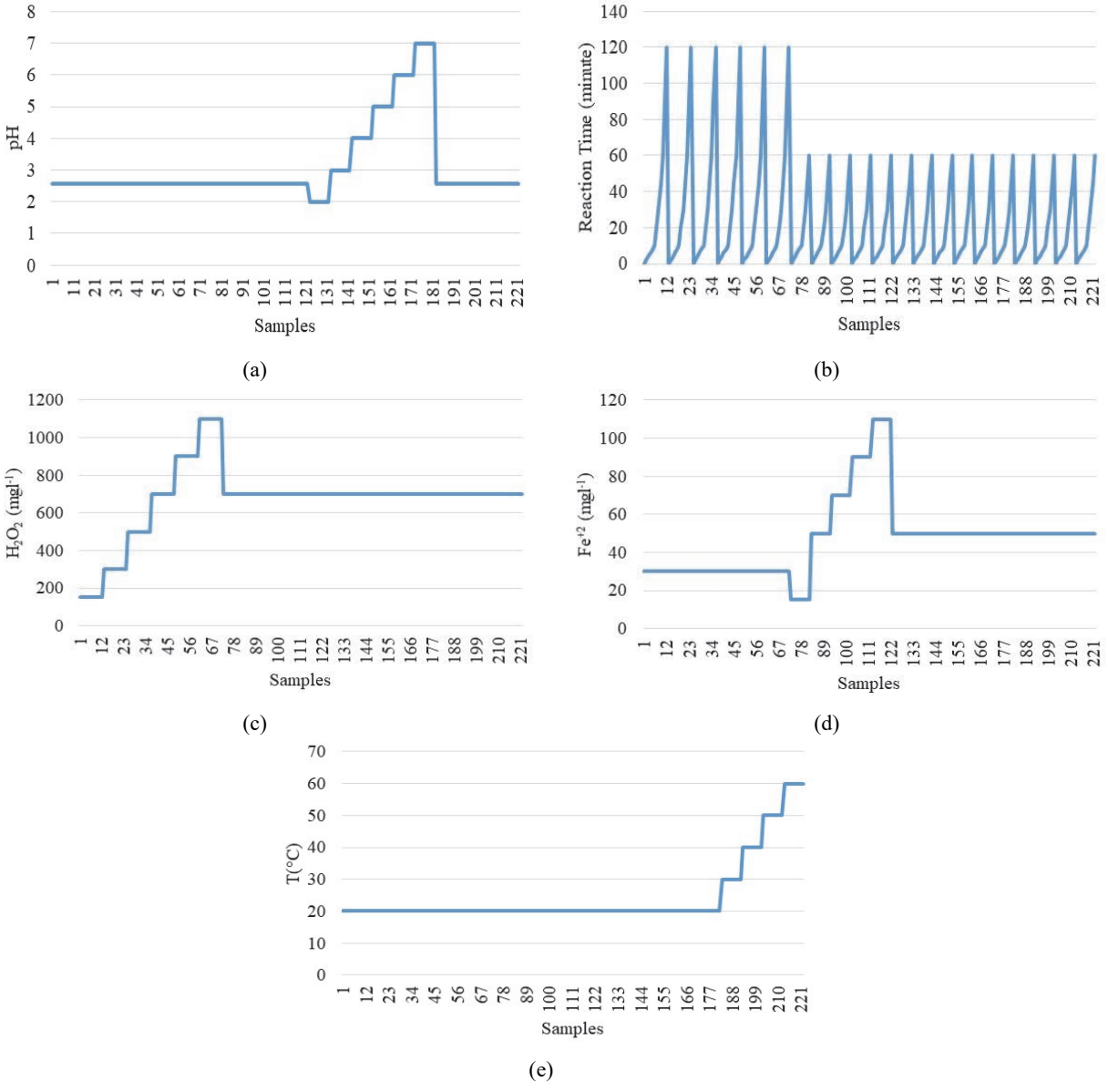

Fig. 3. The range of input parameters: (a) pH, (b) reaction time, (c) H_2O_2, (d) Fe^{2+}, (e) T (°C)

Table 1. Functions and neuron numbers used in the ANNs

Learning function	***Transfer functions***		***Neuron number***
Levenberg-Marquardt (Trainlm)	***Hidden Layer***	***Output Layer***	10
	Logsig	Logsig	
	Tansig	Tansig	
	Pureline	Pureline	15
	Logsig	Tansig	
	Logsig	Pureline	20
	Tansig	Pureline	

Logsig: logarithmic sigmoid, Tansig: Symmetric sigmoid, Pureline: Linear transfer functions

MAE is a measure used to evaluate how close the estimates are to the observed (real) results. The model is also considered accurate when *RMSE* and *MAE* are as small as possible. The acceptable values of *RMSE, MAE* and R^2 mean that the model describes the actual behavior of system accurately.

$$RMSE = \sqrt{\frac{1}{n}\sum_{i=1}^{n}(Y_{pi} - Y_{di})^2} \quad (7)$$

$$MAE = \frac{1}{n}\sum_{i=1}^{n}\left|Y_{pi} - Y_{di}\right| \quad (8)$$

$$R^2 = 1 - \left(\frac{\sum_{i=1}^{n}(Y_{pi} - Y_{di})^2}{\sum_{i=1}^{n}(Y_{pi} - \bar{Y})^2}\right) \quad (9)$$

In these equations; n is the number of observations, Y_{pi} is the model's predicted value of the i^{th} observation from the model constructed, Y_{di} is the real value from observation i, and $\bar{Y}$ is the average of the real value.

2.8. Sensitivity analysis

To appoint how much significant the input parameters are, the weight matrices and Garson equation (Eq. 10) were used (Aleboyeh et al., 2008). In the equation I_j is percentage of the relative importance of the j^{th} input variable on the neurons and W^{ih} and W^{ho} are the matrices of weights between input-hidden layer and hidden-output layer respectively, N is the total number of neurons in the corresponding layer, respectively, and subscripts '*k*', '*m*' and '*n*' are indices referring to the neurons in input, hidden and output layers, respectively.

$$I_j = \frac{\sum_{m=1}^{Nh}\left(\left|w_{jm}^{ih}\right| / \sum_{k=1}^{Ni}\left|w_{km}^{ih}\right|\right)\times\left|w_{mn}^{ho}\right|}{\sum_{k=1}^{Ni}\left\{\sum_{m=1}^{Nh}\left(\left|w_{km}^{ih}\right| / \sum_{k=1}^{Ni}\left|w_{km}^{ih}\right|\right)\times\left|w_{mn}^{ho}\right|\right\}} \quad (10)$$

3. Results and discussion

3.1. Results of 2-CP and $COD_{2\text{-}CP}$

The statistical results of 2-CP and $COD_{2\text{-}CP}$ were given in Table 2. The best results were obtained from the ANN10 structure for 2-CP and $COD_{2\text{-}CP}$. In this structure, the R^2 values were calculated as 0.984 and 0.962 for 2-CP and $COD_{2\text{-}CP}$, respectively. Logarithmic sigmoid - symmetric sigmoid transfer functions with 15 neurons were used in the ANN 10.

Values of coefficient of correlation which were indicated as R in the figures in ANN10 structure for all the training, validation and test sets were determined as greater than 0.99 (Figs.4-5). In addition, the values RMSE and MAE of the ANN10 were lower than the other structures. For these reasons it could be said that the 2-CP and $COD_{2\text{-}CP}$ were forecasted at highly accurate level.

Table 2. The statistical results 2-CP and $COD_{2\text{-}CP}$

Model	***LF***	***TF***	***NN***	***2-CP***			***$COD_{2\text{-}CP}$***		
				RMSE	***MAE***	***R^2***	***RMSE***	***MAE***	***R^2***
ANN 1	Trainlm	L-L	10	0.724	0.622	0.602	0.454	0.359	0.735
ANN 2	Trainlm	T-T	10	0.113	0.074	0.978	0.134	0.100	0.940
ANN 3	Trainlm	P-P	10	0.529	0.422	0.481	0.398	0.311	0.463
ANN 4	Trainlm	L-T	10	0.162	0.105	0.962	0.113	0.083	0.957
ANN 5	Trainlm	L-P	10	0.137	0.102	0.966	0.134	0.093	0.941
ANN 6	Trainlm	T-P	10	0.114	0.086	0.976	0.118	0.082	0.953
ANN 7	Trainlm	L-L	15	0.696	0.557	0.808	0.468	0.390	0.733
ANN 8	Trainlm	T-T	15	0.132	0.082	0.969	0.140	0.076	0.934
ANN 9	Trainlm	P-P	15	0.525	0.417	0.491	0.394	0.303	0.473
ANN 10	Trainlm	L-T	15	0.095	0.065	0.984	0.105	0.074	0.962
ANN 11	Trainlm	L-P	15	0.112	0.081	0.977	0.140	0.099	0.934
ANN 12	Trainlm	T-P	15	0.105	0.073	0.980	0.131	0.091	0.942
ANN 13	Trainlm	L-L	20	0.696	0.555	0.807	0.484	0.397	0.538
ANN 14	Trainlm	T-T	20	0.140	0.090	0.967	0.214	0.157	0.856
ANN 15	Trainlm	P-P	20	0.542	0.411	0.482	0.397	0.302	0.470
ANN 16	Trainlm	L-T	20	0.103	0.069	0.981	0.113	0.078	0.957
ANN 17	Trainlm	L-P	20	0.139	0.105	0.965	0.132	0.093	0.945
ANN 18	Trainlm	T-P	20	0.108	0.078	0.979	0.118	0.075	0.953

Trainlm: Levenberg-Marquardt learning function; L: logarithmic sigmoid, T: symmetric sigmoid, P: linear transfer functions, LF: learning function, TF: transfer functions, NN: neuron numbers

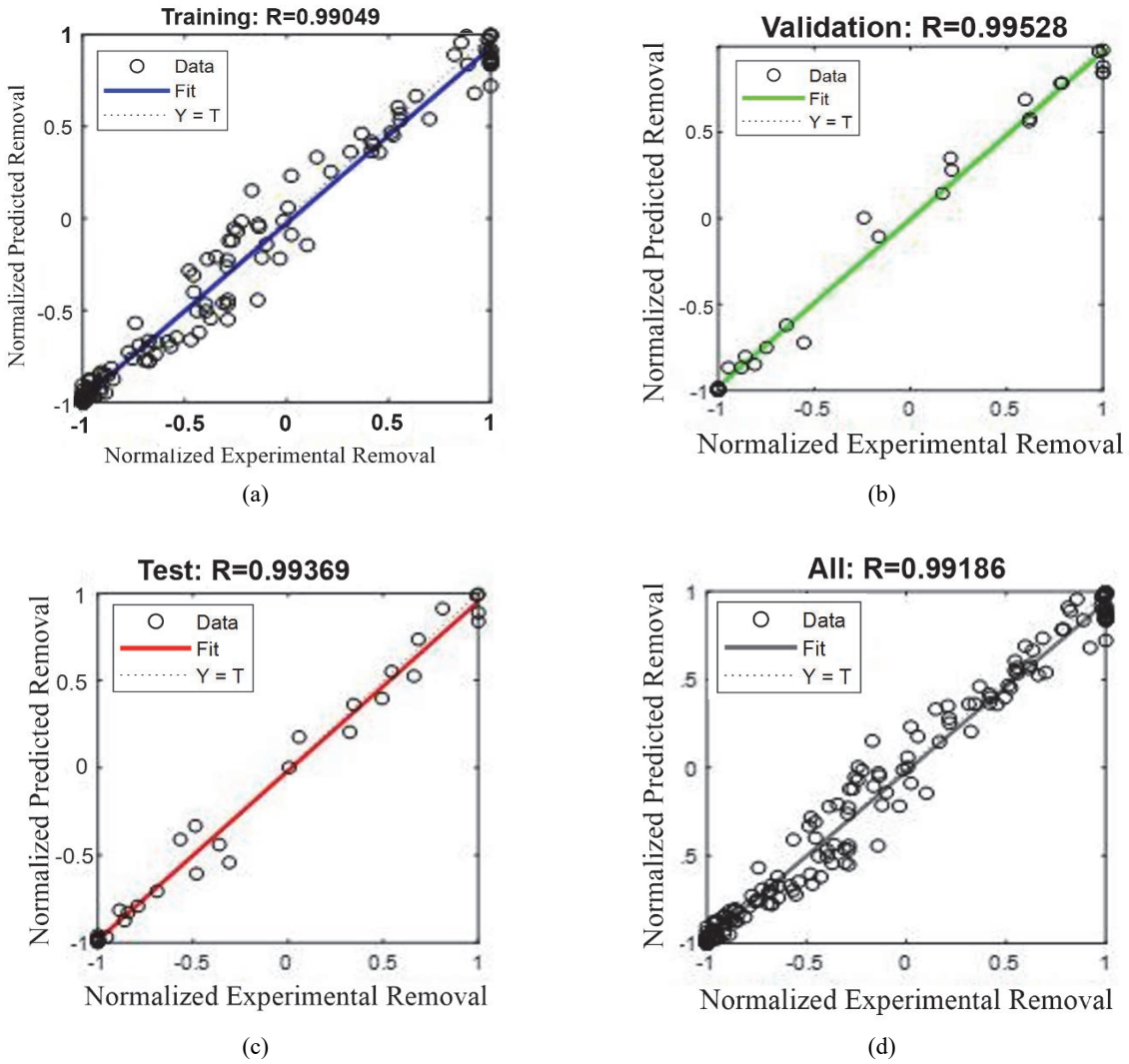

Fig. 4. The network performance of 2-CP at the ANN 10 structure (a) training, (b) validation, (c) test, (d) all

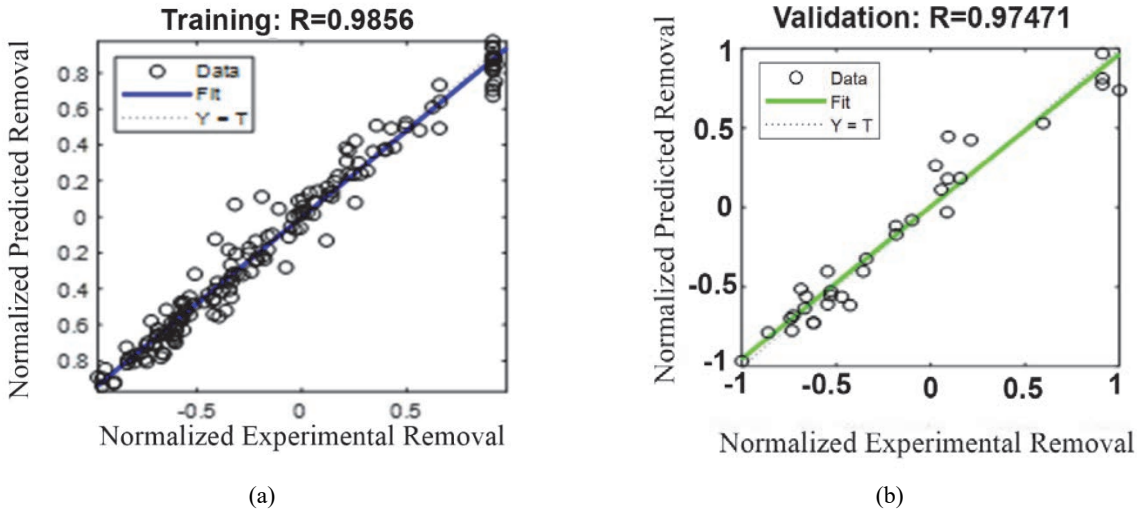

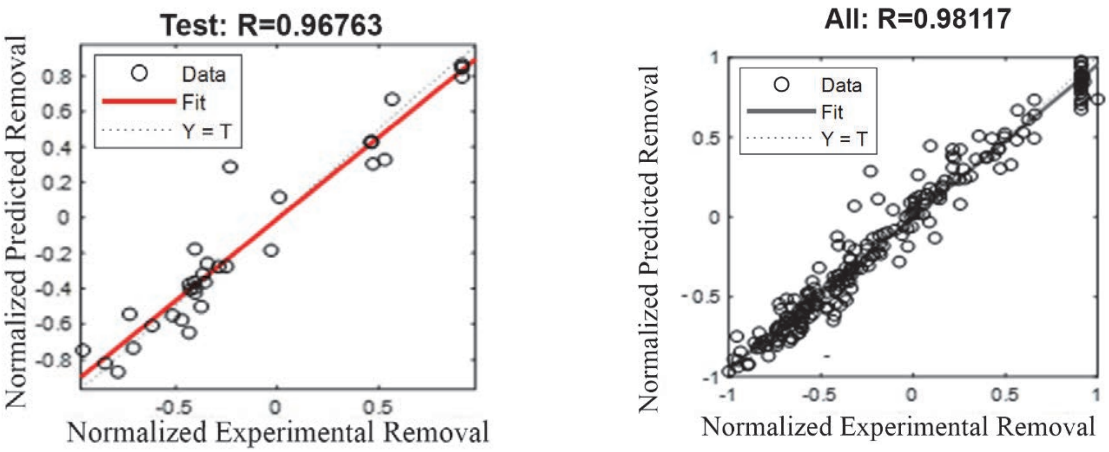

(c) (d)

Fig. 5. The network performance of $COD_{2\text{-}CP}$ at the ANN 10 structure (a) training, (b) validation, (c) test, (d) all

The network performances forecasted values of 2-CP and $COD_{2\text{-}CP}$ were illustrated in Fig. 6.

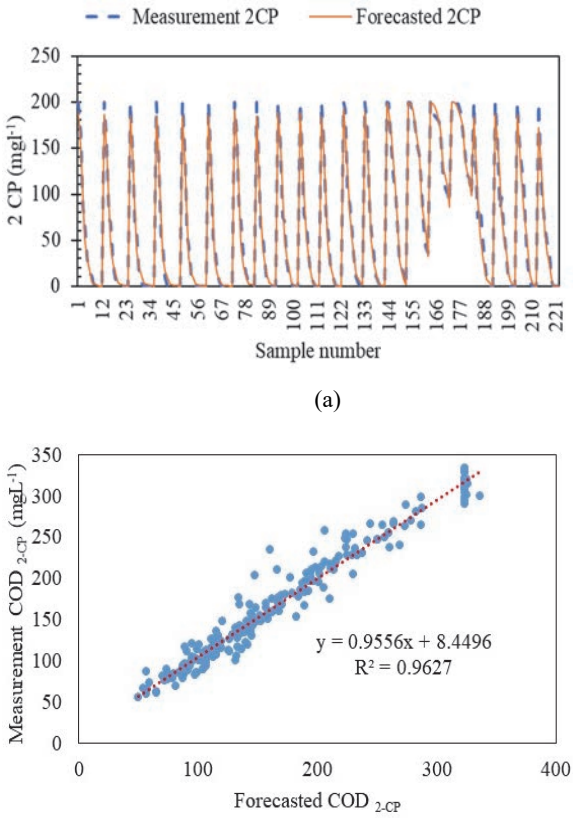

(a)

(b)

Fig. 6. Measurement and Forecasted values at the ANN10 (a) 2-CP, (b) $COD_{2\text{-}CP}$

Tables 3-4 shows the weights of ANN10 structure for 2-CP and $COD_{2\text{-}CP}$, respectively. In addition, the relative importance values of 2-CP and $COD_{2\text{-}CP}$ were illustrated in Fig. 7. The reaction time for both 2-CP and $COD_{2\text{-}CP}$ has high relative importance. Generally, the reaction time was followed by pH, temperature and Fe^{2+}.

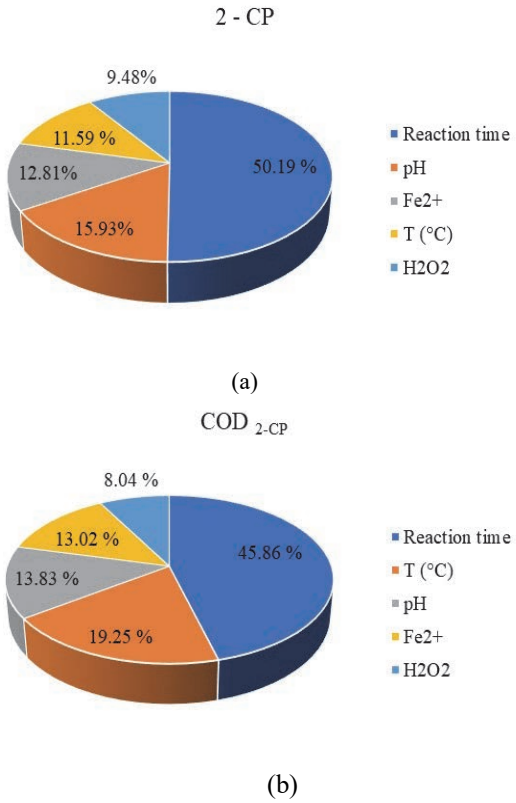

(a)

(b)

Fig. 7. Relative importance values for 2-CP (a) and $COD_{2\text{-}CP}$ (b) at the ANN10 structure

3.2. Results of 2,4-DCP and $COD_{2,4\text{-}DCP}$

Table 5 illustrated the statistical results of 2,4-DCP and $COD_{2,4\text{-}DCP}$ for different ANNs. Unlike the 2-CP and $COD_{2\text{-}CP}$, the best models resulted for in ANN16 and ANN2 structures for 2,4-DCP and $COD_{2,4\text{-}DCP}$. ANN16 model for predicting 2,4-DCP resulted slightly better than ANN2 structure. Examining the statistical results of 2,4-DCP it can be seen that R^2, RMSE and MAE values of ANN16 structure were 0.995, 0.053 and 0.034, respectively.

Table 3. The weights for 2-CP at the ANN10 structure

Neuron number	W^{ih}					W^{ho}
	Inputs					Output
	t (min)	H_2O_2(mg L^{-1})	Fe^{2+} (mg L^{-1})	pH	T (°C)	2-CP(mg L^{-1})
1	-2.867	-1.519	-2.348	-2.623	-0.700	-0.934
2	1.456	-2.958	-1.732	-0.413	-0.092	1.593
3	-2.640	-3.860	-0.027	-0.714	-0.173	-0.685
4	3.922	-1.651	2.323	-1.074	0.284	0.024
5	2.362	1.208	1.737	2.235	2.890	0.495
6	2.241	3.885	-0.057	-0.054	2.987	-1.543
7	3.152	-1.502	1.957	1.138	-0.638	-0.333
8	1.737	0.823	4.281	1.486	3.700	-2.490
9	-1.871	5.155	-0.981	5.530	-0.026	0.960
10	3.155	1.884	0.419	-8.223	3.943	-1.168
11	2.400	-1.271	2.327	2.325	0.172	1.381
12	-2.584	-0.403	-1.329	4.814	-1.714	0.849
13	9.119	-0.421	-4.799	2.604	-3.656	-1.439
14	-11.055	-0.001	0.523	-2.051	-0.911	11.989
15	-7.944	0.115	-2.418	1.315	1.656	5.226

(W^{ih}: input-hidden layer, W^{ho}: hidden-output layer weights)

Table 4. The weights for COD $_{2\text{-CP}}$ at the ANN 10 structure

Neuron number	W^{ih}					W^{ho}
	Inputs					Output
	t (min)	H_2O_2(mg L^{-1})	Fe^{2+}(mg L^{-1})	pH	T (°C)	$COD_{2\text{-CP}}$(mg L^{-1})
1	-4.256	1.410	0.341	-0.557	-0.881	0.6129
2	2.963	0.666	2.680	-0.133	-2.614	1.0842
3	2.473	-0.185	2.178	4.099	-0.530	-1.3210
4	-4.806	-0.293	0.221	0.103	-5.591	2.8286
5	3.270	-0.415	2.186	1.776	2.074	-0.0275
6	0.837	-1.317	1.270	3.875	-2.870	1.8545
7	-1.540	-0.743	3.300	0.084	4.745	-2.7658
8	2.712	0.464	-2.362	3.812	-3.967	-2.8404
9	-0.271	-4.068	1.261	3.934	2.248	2.0945
10	-0.727	0.387	0.706	3.397	3.216	1.8095
11	-3.844	-0.300	-1.355	-3.172	0.170	0.8548
12	2.128	4.606	4.339	0.381	2.848	-1.0953
13	-0.952	-4.492	6.978	2.509	-3.664	-1.4364
14	-21.532	0.129	0.300	-0.080	-0.223	11.2261
15	1.893	1.854	-3.619	-3.058	1.415	1.6597

(W^{ih}: input-hidden layer, W^{ho}: hidden-output layer weights)

Table 5. Statistical results of 2,4-DCP and $COD_{2,4\text{-DCP}}$ at the different ANNs

Model	LF	TF	NN	2,4-DCP			$COD_{2,4\text{-DCP}}$		
				RMSE	MAE	R^2	RMSE	MAE	R^2
ANN 1	Trainlm	L-L	10	0.663	0.512	0.814	0.377	0.262	0.797
ANN 2	Trainlm	T-T	10	0.060	0.040	0.994	0.071	0.051	0.985
ANN 3	Trainlm	P-P	10	0.541	0.449	0.503	0.413	0.335	0.480
ANN 4	Trainlm	L-T	10	0.087	0.060	0.987	0.102	0.075	0.968
ANN 5	Trainlm	L-P	10	0.083	0.062	0.988	0.117	0.089	0.959
ANN 6	Trainlm	T-P	10	0.102	0.069	0.983	0.189	0.149	0.891
ANN 7	Trainlm	L-L	15	0.664	0.514	0.820	0.377	0.262	0.788
ANN 8	Trainlm	T-T	15	0.067	0.046	0.992	0.118	0.085	0.958
ANN 9	Trainlm	P-P	15	0.529	0.450	0.508	0.416	0.338	0.481
ANN10	Trainlm	L-T	15	0.063	0.044	0.993	0.109	0.082	0.965
ANN 11	Trainlm	L-P	15	0.079	0.059	0.989	0.105	0.078	0.967
ANN 12	Trainlm	T-P	15	0.116	0.088	0.976	0.097	0.071	0.972
ANN 13	Trainlm	L-L	20	0.663	0.511	0.820	0.379	0.264	0.771
ANN 14	Trainlm	T-T	20	0.069	0.046	0.992	0.102	0.076	0.968
ANN 15	Trainlm	P-P	20	0.633	0.562	0.340	0.414	0.332	0.481
ANN 16	Trainlm	L-T	20	0.053	0.034	0.995	0.089	0.061	0.976
ANN 17	Trainlm	L-P	20	0.132	0.102	0.970	0.117	0.089	0.958
ANN 18	Trainlm	T-P	20	0.097	0.073	0.984	0.105	0.077	0.966

Trainlm: Levenberg-Marquardt learning function; L: logarithmic sigmoid, T: Symmetric sigmoid, P: Linear transfer functions, LF: learning function, TF: transfer function, NN: Neuron number

The R^2 value at ANN2 for forecasting 2,4-DCP was higher than the others while RMSE and MAE values lower than other ANN structures. This mean that model of forecasting 2,4-DCP was very accurate. The model performance of ANN16 structure that used forecasting 2,4-DCP was given in Fig. 8. When examined the Fig. 8 the R^2 values both training, validation and testing were greater than 0.99. These results were explained that model's high accuracy level. In addition, this high accuracy level can be seen from the Fig. 9. The similar results can be seen from Table 5 for forecasting $COD_{2,4\text{-DCP}}$ values. The higher R^2 and lower RMSE and MAE values for forecasted $COD_{2,4\text{-DCP}}$ were calculated at the ANN2 structure with 0.985, 0.071 and 0.051, respectively. The model performance of ANN2 for forecasting $COD_{2,4\text{-DCP}}$ and measurement - forecasted values were illustrated Figs. 10-11, respectively. The results of sensitivity analysis were given in Tables 6-7 for 2,4-DCP and $COD_{2,4\text{-DCP}}$ respectively and also Fig. 12 illustrates relative importance values for 2,4-DCP and $COD_{2,4\text{-DCP}}$ at the ANN16 and ANN2 structures.

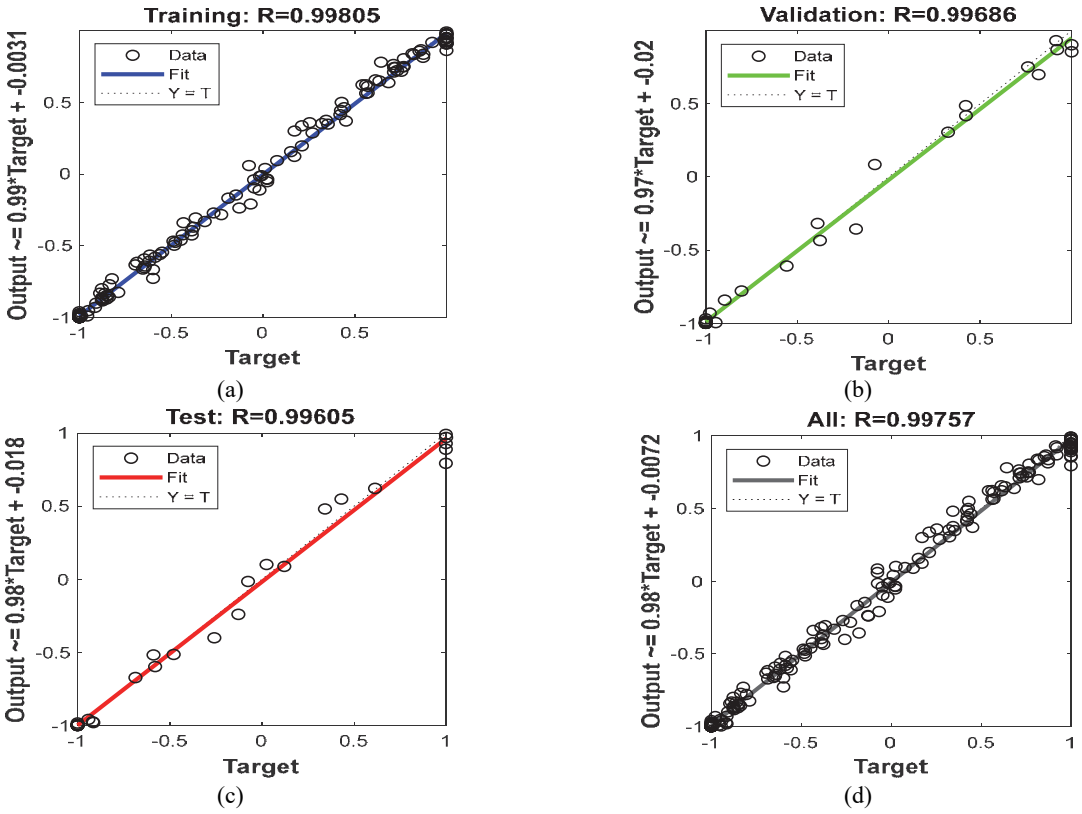

Fig. 8. The network performance of ANN16 structure for forecasting 2,4-DCP: (a) training, (b) validation, (c) test, (d) all

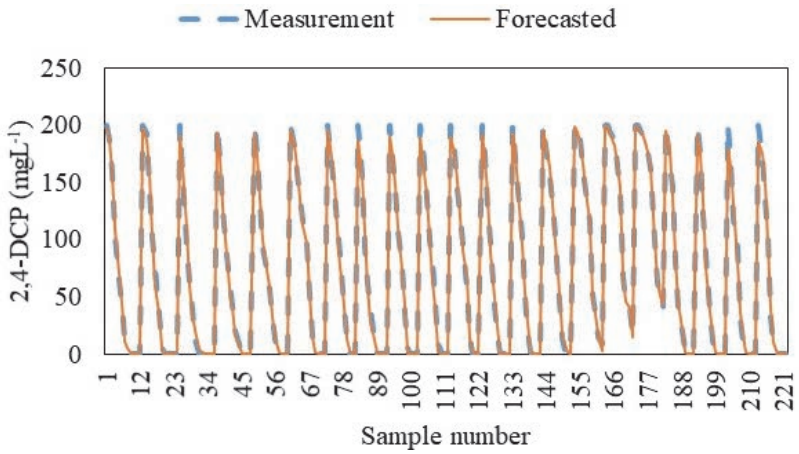

Fig. 9. Measurement and forecasted values of 2,4-DCP at the ANN 16 structure

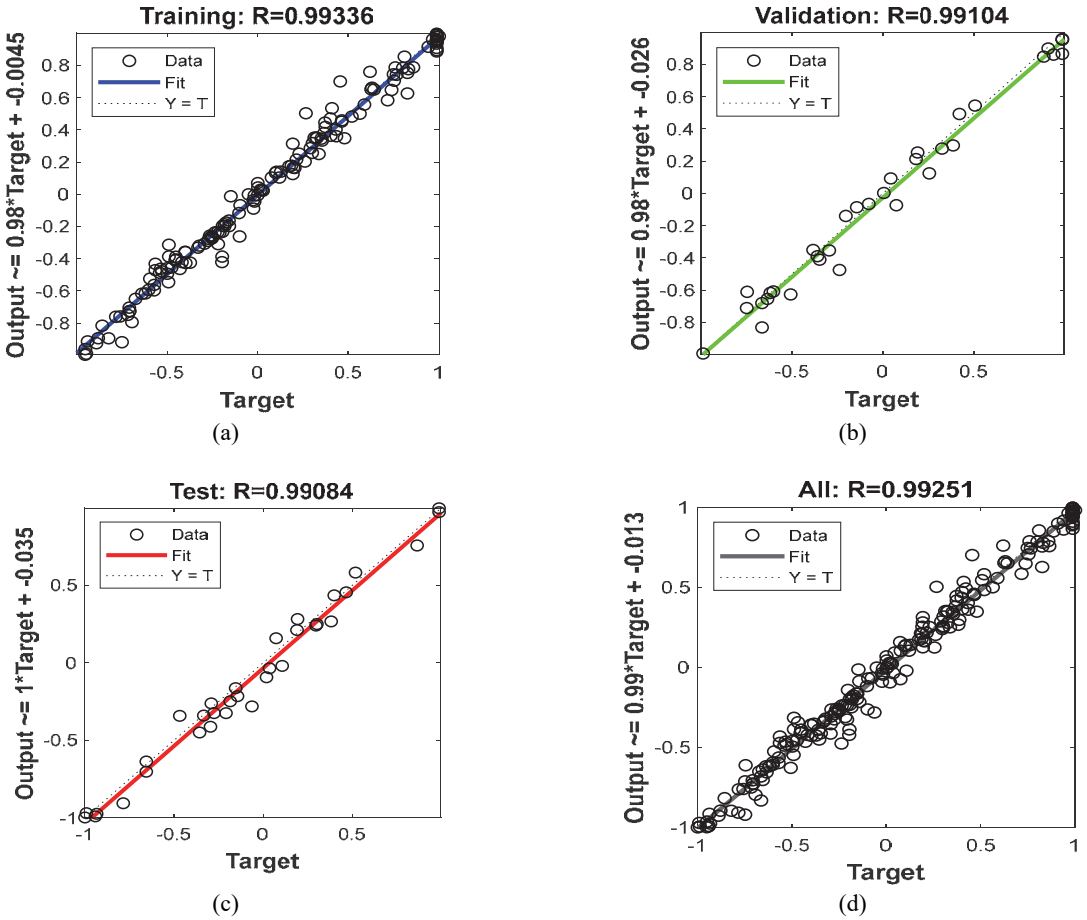

Fig. 10. The network performance of ANN2 for forecasting COD $_{2,4\text{-DCP}}$ (a) training, (b) validation, (c) test, (d) all

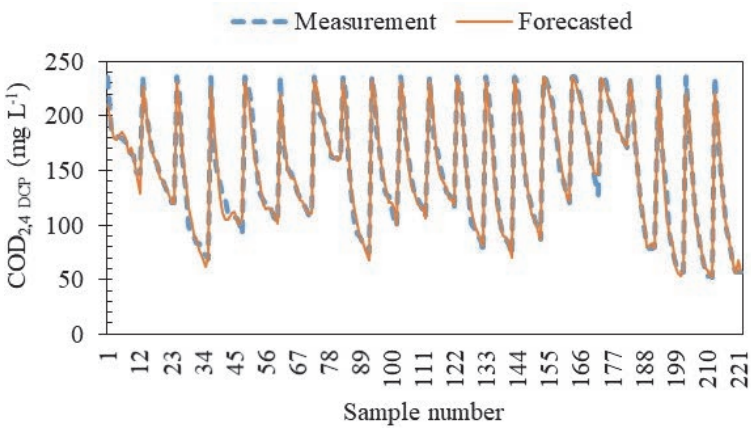

Fig. 11. Measurement and forecasted values of COD$_{2,4\text{-DCP}}$ at the ANN2 structure

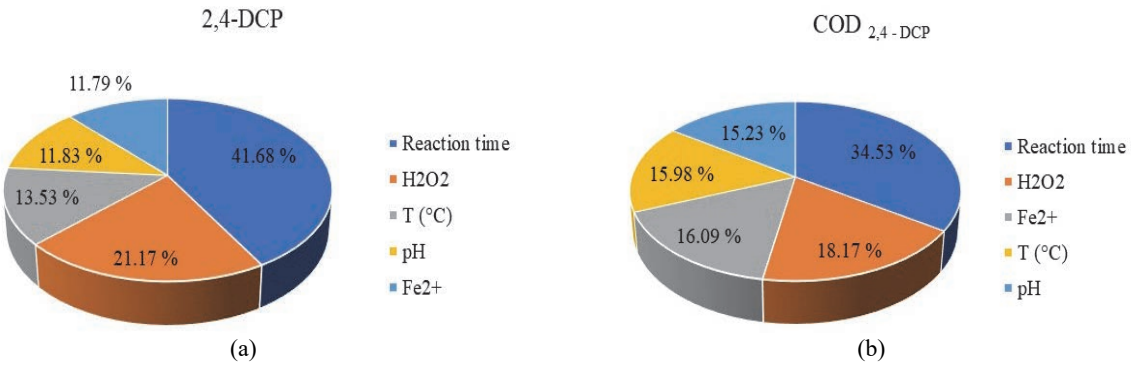

Fig. 12. Relative importance values for 2,4-DCP (a) and COD$_{2,4\text{-DCP}}$ (b) at the ANN16 and ANN2 structures

Table 6. The weights for 2,4-DCP at the ANN16 structure (W^{ih}: input-hidden layer, W^{ho}: hidden-output layer weights)

Neuron number	***W^{ih}***					***W^{ho}***
	Inputs					***Output***
	t (min)	***H_2O_2(mg L^{-1})***	***Fe^{2+}(mg L^{-1})***	***pH***	***T (°C)***	***2,4-DCP(mg L^{-1})***
1	1.5728	0.5483	0.1845	-2.4820	-2.1893	-1.0219
2	0.8611	-2.2170	0.1580	-0.0223	-0.1183	-1.3979
3	-3.1233	-0.2677	0.3545	-0.4329	1.8415	-2.4554
4	1.4685	-1.0516	0.6034	0.9012	-0.9932	-0.5164
5	-0.0012	2.9035	-0.6594	1.6421	-0.7666	-1.6772
6	-3.6915	-0.3443	1.3436	-0.0873	-0.0107	2.4543
7	-1.1496	-1.8832	-0.3832	0.9134	-1.1667	0.9051
8	2.0899	-0.6368	0.2709	0.2555	0.1260	-4.2671
9	1.1671	-0.7705	-0.4186	-0.3602	-1.4415	-0.1539
10	-0.6516	-0.2930	1.9815	-1.3796	1.6579	-1.1347

Table 7. The weights for COD $_{2,4\text{-DCP}}$ at the ANN2 structure (W^{ih}: input-hidden layer, W^{ho}: hidden-output layer weights)

Neuron number	***W^{ih}***					***W^{ho}***
	Inputs					***Output***
	t (min)	***H_2O_2(mg L^{-1})***	***Fe^{2+}(mg L^{-1})***	***pH***	***T (°C)***	***COD $_{2,4\text{-DCP}}$(mg L^{-1})***
1	-0.9095	-0.9532	0.5123	-1.3788	-0.8253	0.7205
2	0.0316	-0.1517	0.8926	-1.8789	-0.1036	0.6059
3	1.1784	-1.0064	0.5225	1.5802	-0.5905	-0.6412
4	-0.2520	2.3216	2.2209	-0.2573	-0.7303	1.0017
5	0.1574	-1.3443	-1.6222	1.0794	0.4132	1.8842
6	-1.5573	-1.6702	0.2488	-0.7606	0.7308	-0.1390
7	1.6332	2.2986	-0.9668	-0.2173	-1.8185	1.4067
8	0.6891	0.2968	0.5245	-1.0857	-1.9121	1.1156
9	-5.8290	-0.1958	0.0511	-0.0371	0.6322	3.1673
10	-1.4333	-0.8695	0.3537	-0.4761	1.7242	0.1224

Artificial neural network was used at the environmental studies, for example; in a research which aimed of modelling of photo-Fenton degradation of Reactive Blue 4 with neural networks (Durán et al., 2006).They used initial concentrations values of Fe^{2+}, H_2O_2, pH, temperature, and RB4 as an input parameter, and decolorization and mineralization kinetic rate constants as an output parameter at the neural networks (NNs). They determined the best values of kinetic constants from the NNs fittings as a result. In another study an ANN model of forecasting of discoloration performance was developed for peroxi - coagulation processes, and the discoloration efficiency were modelled with ANN at the high accuracy level (Salari et al., 2009). Another study used the ANN for the modelling of biotreatment of Malachite Green (MG) solution. For this purpose, the temperature, pH, initial dye concentration, reaction time and number of algae on biological decolorization were used as input parameters. When examined the obtained results, it was seen that the ANN provided reasonable performance ($R^2 = 0.987$) and, can estimate the behavior of the biological biotreatment process (Khataee et al., 2011).

In this study, the first aim was to determine the best linear and transfer functions and neuron numbers, the second is determination of the relative importance among the input parameters for substituted phenols removing. For this reason, the researchers focused on the factors of the samples; studied on prediction and simulation research for antibiotic degradation by the Fenton process (Elmolla et al., 2010). For this purpose, the ANN method was used, and they observed the best simulation values at the backpropagation neural network with Tansig at hidden layer with 14 neurons, Pureline at output layer and Levenberg-Marquardt backpropagation training algorithm (Trainlm). ANN method was used for forecasting the decolorization of C.I. direct red 16 (DR16) using UV/$K_2S_2O_8$ process. When examined the results, the best result was obtained at the three-layered ANN, and in this ANN structure it was used BFGS quasi-Newton backpropagation learning function, Tansig and Pureline as transfer functions in hidden and output layers (Soleymani et al., 2011).

At another work, implementation of ANN was studied for predicting and simulating oil degradation in aqueous solution by photo-Fenton process. According to the results, the best simulation values were determined from backpropagation algorithm which has a three-layer network with 22 neurons in each hidden layer (Mustafa et al., 2014).

As in the other studies, in this study, the determination of the ANN models that may be used in the removal of substituted phenols by advanced oxidation techniques was researched. In addition, the sensitivity analyses were applied to the input parameters and their effect levels were determined.

4. Conclusions

In this research it was aimed to forecast 2-CP, $COD_{2\text{-}CP}$, 2,4-DCP and $COD_{2,4\text{-}DCP}$ of AOPs with ANN. For this purpose, 18 different ANN structures were used. One learning function, six different transfer function combinations and three different neuron numbers were used at these structures. In addition, the sensitivity analyses were implemented to designate the effects of input parameters on removal procedures.

Values for 2-CP, $COD_{2\text{-}CP}$, 2,4-DCP and $COD_{2,4\text{-}DCP}$ were predicted with ANN successfully. The best results for prediction of 2-CP and $COD_{2\text{-}CP}$ were obtained from ANN10 structure which has Trainlm, Logsig-Tansig transfer function with 15 neuron number. The R^2 values of this structure were calculated as 0.984 and 0.962 for 2-CP and $COD_{2\text{-}CP}$, respectively. The ANN16 and ANN2 models, which were used for the prediction of and 2,4-DCP and $COD_{2,4\text{-}DCP}$, has obtained better results than the other models. ANN16 model used Levenberg-Marquardt and Logsig-Tansig for learning and transfer functions with 20 neuron number, respectively. The ANN2 model used Levenberg-Marquardt and Tansig-Tansig for learning and transfer functions with 10 neuron number, respectively.

Finally, R^2 values were determined as 0.995 and 0.985 for prediction of 2,4-DCP and $COD_{2,4\text{-}DCP}$, respectively. The sensitivity analyses showed that all of the input parameters have a significant effect on the removing AOPs procedures.

References

Aber S., Daneshvar N., Soroureddin S.M., Chabok A., Asadpour-Zeynali K., (2007), Study of acid orange 7 removal from aqueous solutions by powdered activated carbon and modeling of experimental results by artificial neural network, *Desalination*, **211**, 87-95.

Aleboyeh A., Kasiri M.B., Olya M.E., Aleboyeh H., (2008), Prediction of azo dye decolorization by UV/H_2O_2 using artificial neural networks, *Dyes and Pigments*, **77**, 288-294.

Alyani S.J., Pirbazari A.E., Khalilsaraei F.E., Kolur N.A., Gilani N., (2019), Growing Co-doped TiO_2 nanosheets on reduced graphene oxide for efficient photocatalytic removal of tetracycline antibiotic from aqueous solution and modeling the process by artificial neural network, *Journal of Alloys and Compounds*, **799**, 169-182.

Ameta R., Chohadia A.K., Jain A., Punjabi P.B., (2018), - *Fenton and Photo-Fenton Processes*, In: *Advanced Oxidation Processes for Waste Water: Treatment*: *Emerging Green Chemical Technology*, Ameta S., Ameta R. (Eds.), Academic Press, New York, 49-87.

Ameta S.C., (2018), *Introduction*, In: *Advanced Oxidation Processes for Waste Water Treatment*: *Emerging Green Chemical Technology*, Ameta S.C., Ameta R. (Eds.), Academic Press, New York, 1-12.

APHA, (2017), Standard methods for examination of water and wastewater, American Public Health Association, On line at: https://www.standardmethods.org/doi/10.2105/SMWW.2882.103.

Badanthadka M., Mehendale H.M., (2014), *Chlorophenols, Reference Module in Biomedical Sciences,* In: *Encyclopedia of Toxicology*, 3rd Edition, Academic Press, New York, 896-899.

Bautista P., Mohedano A.F., Gilarranz M.A., Casas J.A., Rodriguez J.J., (2007), Application of Fenton oxidation to cosmetic wastewaters treatment, *Journal of Hazardous Materials*, **143**, 128-134.

Daneshvar N., Khataee A.R., Djafarzadeh N., (2006), The use of artificial neural networks (ANN) for modeling of decolorization of textile dye solution containing C.I. Basic Yellow 28 by electrocoagulation process, *Journal of Hazardous Materials*, **137**, 1788-1795.

Duesterberg C.K., Mylon S.E., Waite T.D., (2008), pH effects on iron-catalyzed oxidation using Fenton's reagent, *Environmental Science and Technology*, **42**, 8522-8527.

Durán A., Monteagudo J.M., Mohedano M., (2006), Neural networks simulation of photo-Fenton degradation of Reactive Blue 4, *Applied Catalysis B: Environmental*, **65**, 127-134.

Elmolla E.S., Chaudhuri M., Eltoukhy M.M., (2010), The use of artificial neural network (ANN) for modeling of COD removal from antibiotic aqueous solution by the Fenton process, *Journal of Hazardous Materials*, **179**, 127-134.

Gulkaya I., Surucu G., Dilek F., (2006), Importance of H_2O_2/Fe^{2+} ratio in Fenton's treatment of a carpet dyeing wastewater, *Journal of Hazardous Materials*, **136**, 763-769.

Igbinosa E.O., Odjadjare E.E., Chigor V.N., Igbinosa I.H., Emoghene A.O., Ekhaise F.O., Igiehon N.O., Idemudia O.G., (2013), Toxicological profile of chlorophenols and their derivatives in the environment: The Public health perspective, *The Scientific World Journal*, **2013**, 1-11.

Kavitha V., Palanivelu K., (2004), The role of ferrous ion in Fenton and photo-Fenton processes for the degradation of phenol, *Chemosphere*, **55**, 1235-1243.

Khataee A.R., Dehghan G., Zarei M., Ebadi E., Pourhassan M., (2011), Neural network modeling of biotreatment of triphenylmethane dye solution by a green macroalgae, *Chemical Engineering Research and Design*, **89**, 172-178.

Klassen N.V., Marchington D., McGowan H.C.E., (1994), H_2O_2 determination by the I3- Method and by $KMnO_4$ titration, *Analytical Chemistry*, **66**, 2921-2925.

Kundu P., Debsarkar A., Mukherjee S., (2013), Artificial neural network modeling for biological removal of organic carbon and nitrogen from slaughterhouse wastewater in a sequencing batch reactor, *Advances in Artificial Neural Systems*, ID 268064, https://doi.org/10.1155/2013/268064.

Lathasree S., Rao A.N., Sivasankar B., Sadasivam V., Rengaraj K., (2004), Heterogeneous photocatalytic mineralisation of phenols in aqueous solutions, *Journal of Molecular Catalysis A: Chemical*, **223**,101-105.

Moral H., Aksoy A., Gokcay C.F., (2008), Modeling of the activated sludge process by using artificial neural networks with automated architecture screening, *Computers & Chemical Engineering*, **32**, 2471-2478.

Mustafa Y.A., Jaid G.M., Alwared A.I., Ebrahim M., (2014), The use of artificial neural network (ANN) for the prediction and simulation of oil degradation in wastewater by AOP, *Environmental Science and Pollution Research*, **21**, 7530-7532.

Nesheiwat F.K., Swanson A.G., (2000), Clean contaminated sites using Fenton's reagent, *Chemical Engineering Progress*, **96**, 61-66.

Oguz E., Tortum A., Keskinler B., (2008), Determination of the apparent rate constants of the degradation of humic substances by ozonation and modeling of the removal of humic substances from the aqueous solutions with neural network, *Journal of Hazardous Materials*, **157**, 455-463.

Olaniran A.O., Igbinosa E.O., (2011), Chlorophenols and other related derivatives of environmental concern: Properties, distribution and microbial degradation processes, *Chemosphere*, **83**, 1297-1306.

Pareek V.K., Brungs M.P., Adesina A.A., Sharma R., (2002), Artificial neural network modeling of a multiphase photodegradation system, *Journal of Photochemistry and Photobiology A: Chemistry*, **149**, 139-146.

Pawul M., Śliwka M., (2016), Application of artificial neural networks for prediction of air pollution levels in environmental monitoring, *Journal of Ecological Engineering*, **17**, 190-196.

Prakash N., Manikandan S.A., Govindarajan L., Vijayagopal V., (2008), Prediction of biosorption efficiency for the removal of copper(II) using artificial neural networks, *Journal of Hazardous Materials*, **152**, 1268-1275.

Reitberger T., (2001), *Involvement of Oxygen-Derived Free Radical in Chemical and Biochemical Degradation of Lignin*, In: *Oxidative Delignification Chemistry; Fundamentals and Catalysis*, Argyropoulos D.S. (Ed.), Edition: ACS Symposium Series 785, American Chemical Society, 255-271.

Rodríguez A., Rosal R., Perdigón-Melón J.A., Mezcua M., Agüera A., Hernando M.D., Letón P., Fernández-Alba A.R., García-Calvo E., (2008), *Ozone-Based Technologies in Water and Wastewater Treatment*, In: *Emerging Contaminants from Industrial and Municipal Waste*, vol. 5, Springer-Verlag, Heidelberg, Berlin, 127-175.

Salari D., Niaei A., Khataee A., Zarei M., (2009), Electrochemical treatment of dye solution containing C.I. Basic Yellow 2 by the peroxi-coagulation method and modeling of experimental results by artificial neural networks, *Journal of Electroanalytical Chemistry*, **629**, 117-125.

Soleymani A.R., Saien J., Bayat H., (2011), Artificial neural networks developed for prediction of dye decolorization efficiency with UV/$K_2S_2O_8$ process, *Chemical Engineering Journal*, **170**, 29-35.

Strik D., Domnanovich A.M., Zani L., Braun R., Holubar P., (2005), Prediction of trace compounds in biogas from anaerobic digestion using the MATLAB Neural Network Toolbox, *Environmental Modelling & Software*, **20**, 803-810.

Tengrui L., Al-Harbawi A., Jun Z., Bo L.M., (2007), The effect and its influence factors of the Fenton process on the old landfill leachate, *Journal of Applied Sciences*, **7**, 724-727.

Zak S., (2008), Problem of correction of the chemical oxygen demand values determined in wastewaters treated by methods with hydrogen peroxide, *Proceedings of ECOpole*, **2**, 409-414.

Zhao X.K., Yang G.P., Wang Y.J., Gao X.C., (2004), Photochemical degradation of dimethyl phthalate by Fenton reagent, *Journal of Photochemistry and Photobiology A: Chemistry*, **161**, 215-220.